Available Online: 16 November 2026 DOI: 10.54254/2977-3903/2026.39220

Cooling tower frequency optimization and energy saving potential in a tobacco factory chiller plant with a fixed equipment combination

***Feng Zeng*[1], *Wang Ruan*[1], *Hongyu Gu*[1], *Hehua Shao*[1], *Yanqin Han*[1], *Rui Rong*[2], *Jing Wang*[1,*]**

[1]Baoding Cigarette Factory of Hebei Baisha Tobacco Co., Ltd., Baoding, China
[2]Hebei Province Key Laboratory of Low-Carbon High-Efficiency Power Generation Technology, North China Electric Power University, Baoding, China

*Corresponding Author. Email: bdwj881111@126.com

Abstract. Tobacco manufacturing requires a continuous and stable cooling source for process air conditioning. Chiller-plant optimization must reduce refrigeration and heat-rejection electricity while preserving the established cooling service. In operating archives from industrial plants, however, tower frequency, condenser-water temperature and existing feedback actions often change together, so historical association alone does not identify the temperature response to a new frequency. This study addresses that problem for a tobacco factory chiller plant in Yangzhou by formulating a component energy balance for a fixed equipment combination and treating the unmeasured tower-frequency response as an explicit scenario parameter. The archive ending at 00:00 on 15 October 2026 yields 1372 disjoint windows; the primary combination provides 314 windows over 43 operating dates, divided into 279 fitting, 15 validation and 20 evaluation windows. With measured condenser inlet temperature, evaluation RMSE values are 11.24 kW for chiller power and 0.89 kW for tower power. Reducing three towers from 50 to 47.5 Hz gives a modeled fan-power credit of 4.14 kW; at loads of 2,500–4,500 kW, the corresponding break-even warming is 0.130–0.072 °C. Under four specified thermal-response scenarios, local optimization gives mean modeled credits of 0.55–10.50 kW, or 0.10%–1.95% of the accounting boundary, and the preferred direction changes with response intensity. The study quantifies the energy tradeoff and the temperature-response measurements required for a subsequent frequency-adjustment test; the scenario credits are not field-measured savings.

Keywords: tobacco factory, chiller plant, cooling tower frequency, component energy balance, energy saving potential

1. Introduction

Tobacco manufacturing places sustained demands on process air conditioning. Research on cigarette factory temperature and humidity decoupling [1] and workshop air distribution [2] illustrates the connection between environmental regulation and production conditions. A central chiller plant provides the cooling source for

Copyright: © 2026 by the authors. Submitted for possible open access publication under the terms and conditions of the Creative Commons Attribution (CC BY) license (https://creativecommons.org/licenses/by/4.0/).

those air handling systems, so its operating optimization must preserve the downstream cooling service. In this setting, the direct energy target is the electricity used by refrigeration, condenser-water transport and heat rejection. Cooling-tower frequency is therefore a constrained chiller–cooling-side coordination problem rather than a fan-power minimization problem.

Supervisory HVAC optimization coordinates equipment whose individual efficiencies interact [3]. In a condenser water loop, raising cooling tower fan frequency can increase fan electricity while reducing condenser inlet water temperature and chiller electricity. Lower frequency can reverse that exchange. Lu et al. studied optimization of the condenser water loop [4], and Jin et al. developed a simplified mechanical cooling tower model for HVAC control and optimization [5]. More recent work considers systems with variable speed pumps and tower fans [6]. These studies establish that tower electricity alone is an insufficient objective, but many results rely on equipment models, simulation environments or experiments with active excitation. In a plant archive without deliberate perturbations, tower frequency and condenser-water temperature may be jointly determined by an existing feedback controller, so their association need not represent the response to a frequency change. When pump variation is much smaller than tower variation, joint pump–tower optimization also expands the response-identification problem. Two practical questions therefore arise first: can the tower-frequency fan credit cover the chiller penalty within a fixed equipment combination, and does the archive identify the required temperature response?

Recent work addresses the control variables and physical coupling more directly. Online optimization based on a cooling-tower heat-transfer model [7] connects the tower model to cooling-water operation. A 2025 study of variable-speed condenser pumps and tower fans uses derivative-based coordination and reports simulation and experimental checks of the direct control implementation [8]. In that study, the total power derivative with respect to flow is central to the optimization logic. Consequently, balancing marginal fan and chiller power is established engineering reasoning. The present study uses that reasoning to derive a case-specific allowable warming and to expose its sensitivity to a thermal response that the archive does not identify.

The choice of a tower model requires care. Simplified evaporative tower models [9] and analyses of cooling tower exergy optimization [10] represent heat rejection through different levels of physical detail. Stochastic bi-objective optimization for a closed wet cooling tower [11] also treats uncertainty within an analytical model, although its configuration is distinct from the present plant loop. Recent cooling-tower modeling explicitly addresses holistic, dynamic and explainable representations [12]. Such models can guide an energy balance, but their fitted parameters and operating assumptions must match the equipment and observations under study. For a production archive, apparent frequency sensitivity can also contain the behavior of an existing feedback controller: fans may accelerate because water is warm. Consequently, a positive association between recorded frequency and water temperature need not describe the temperature change caused by a frequency command. A physical sign restriction alone does not supply the missing intervention information.

Physical priors and data-driven control provide further relevant comparisons. A physics-informed neural-network study considers structure and trend priors for chiller-plant optimal control [13]. A global self-optimizing control study identifies a nonlinear model from operating data, derives a static input-output map and evaluates controlled-variable selection using a Modelica chilled-water plant model [14]. Its manipulated inputs include tower fan speed and condenser-water flow, making it a close conceptual comparator. The present work does not benchmark against that controller because no independently validated dynamic emulator for this tobacco plant is available. Instead, the comparison clarifies the narrower evidence supplied

here, namely observed-state component fits and conditional local calculations. Physical sign restrictions and an analytical minimum constrain the calculation; the missing thermal response still requires measurement.

Model predictive control provides a broader framework for coordinating dynamics and constraints. Reviews by Afram and Janabi-Sharifi [15], Killian and Kozek [16], and Drgoňa et al. [17] discuss the modeling and implementation demands of building control. Recent chiller research also integrates prediction uncertainty into stochastic optimization [18]. Predictive optimization with a water-side economizer [19] and a recent review of chiller sequencing and optimal loading [20] cover additional plant decisions. Those decisions remain outside this fixed-combination frequency problem. However, a static operating map, a one step forecast and a validated closed loop controller answer different questions. The present work calculates local operating tradeoffs and keeps static fitting, predictive control and alternative-frequency response as separate evidence levels.

The distinction between prediction and explanation discussed by Shmueli [21] is relevant to this setting. System identification likewise requires attention to excitation, model structure and the available operating regime [22]. Research on closed-loop HVAC identification explicitly designs informative inputs and tests the resulting local controllers on an HVAC test bed [23]. Plant and disturbance identification under regulatory control provides a related process-control route [24]. These references support examining the excitation and feedback conditions rather than treating observation count as sufficient. A large number of six minute observations can still contain little useful excitation if the same fans remain near their upper frequency for most fitting dates. Under that condition, a numerical optimizer may find a minimum simply because the estimated thermal penalty is too weak. Treating this minimum as a verified saving would confuse an uncertain model feature with an equipment response. The issue persists even when the optimizer uses a sophisticated search algorithm.

Energy savings assessment introduces a further requirement: an appropriate comparison. Research on inverse modeling for chiller measurement and verification [25] and Gaussian process methods for building savings assessment [26] concerns the construction and uncertainty of such comparisons. Recent field-case chiller-plant optimization research [27] further illustrates that field evaluation is a distinct evidence category. Industrial air-conditioning optimization based on energy prediction has also been examined for a semiconductor factory make-up air unit [28]. That adjacent application supports the broader industrial context, but neither its process requirements nor its reported gains are transferred to tobacco manufacturing. Simulation benchmarks such as BOPTEST provide another route when a suitable plant emulator is available [29]. In the present archive, no independent emulator or controlled tower frequency crossover experiment has been verified. A comparison within the same fitted model can therefore measure conditional optimization potential, but it cannot measure the electricity that the real plant would have consumed under an unobserved alternative policy.

This study addresses a specific problem: for fixed equipment, cooling load and weather context, how can component power relations quantify the energy balance of a tower-frequency change, and what water-temperature evidence is needed before the calculation can support an operating decision? Data are split by date within the same equipment combination to fit and evaluate chiller and fan relations. The fan credit is then converted into an allowable condenser-water warming, and local frequency is solved under specified thermal-response scenarios and compared with fixed-direction policies. The contribution is a case-specific energy boundary, response sensitivity and measurement target that can be checked before a closed-loop optimization study.

2. Plant and observed data

2.1. System boundary and measurements

The plant serves a tobacco factory in Yangzhou and contains three chillers, three cooling towers, three condenser water pumps and three chilled water pumps. The primary operating combination uses chillers 1 and 2, all three towers, condenser pumps 1 and 3, and chilled water pumps 1 and 2. Equipment switches remain fixed in the local optimization. The studied decision is a common tower fan frequency; pump frequency and the chiller internal control are not optimized.

The power accounting boundary is

$$P_b = P_c + P_f + P_{cw}. \tag{1}$$

Here, P_c, P_f and P_{cw} denote measured aggregate chiller, tower fan and condenser pump power. Chilled water pump power is excluded consistently. Since pump settings remain fixed, condenser pump power is held at its observed window value in each scenario. This is a local modeling assumption, not a verified statement that pump electricity is invariant to every thermal change. Percentage improvements refer to Equation (1), not to total factory electricity or the complete plant including chilled water pumps.

The retained archive has a six minute grid and ends at 00:00 on 15 October 2026, inclusive, in the Asia/Shanghai time zone. It contains outdoor conditions, water temperatures, flows, cooling load, equipment states, achieved frequencies and component powers. Wet-bulb temperature is an existing derived archive field; the underlying approximation is associated with the formulation of Stull [30]. Required cells must have direct observation flags. Missing or interpolated required cells do not enter the component fitting samples. Achieved frequency telemetry is an operating observation and is not treated as a time stamped command record. Inactive drives can retain stale frequency values; their effective frequency is set to zero using the measured switch state.

2.2. Window construction and chronological separation

Six consecutive observations span 30 minutes. A qualifying window has the same equipment combination throughout, a cooling load range no greater than 10% of its mean, a wet-bulb temperature range no greater than 0.5 °C and an achieved frequency range no greater than 0.5 Hz for each operating actuator. Cooling load and condenser flow must be positive, at least one chiller and tower must operate, and condenser inlet temperature must exceed wet-bulb temperature by more than 0.1 °C. Existing physical and observation flags are applied before window selection. The rules describe approximately stationary observations; they do not establish a measured tower settling time.

Qualifying windows are selected without overlapping source observations. The archive contains 68881 grid rows, 52567 complete directly observed records under the required fields and 47293 eligible operating records before the window screen. The screen yields 1372 disjoint windows. The primary combination is the only combination with at least 100 windows and a mean tower frequency standard deviation of at least 1 Hz. This selection is descriptive and uses the available archive to define an exploratory case. It is not a prospective case selection or a claim that all equipment combinations share the resulting parameters.

The primary case provides 314 windows over 43 operating dates from 6 August to 28 September. Operating dates are sorted, with the first 60% used for fitting, the next 20% for validation and the remainder for evaluation. The resulting sample counts are unequal because the number of qualifying windows varies by date. The split and action ranges appear in Table 1. Later dates are not used to fit component coefficients. The

archive has already been examined in earlier analyses; the evaluation is therefore a retrospective chronological separation.

Table 1. Primary case windows and achieved mean tower frequencies

Subset	Operating dates	Windows	Date range in 2026	Frequency range Hz
Fitting	25	279	6 Aug to 3 Sep	47.824–50.000
Validation	9	15	4 Sep to 16 Sep	37.715–50.000
Evaluation	9	20	17 Sep to 28 Sep	42.153–50.000

Figure 1 presents the study framework. Figure 2 shows the primary case conditions, frequency excitation shift and sample availability. The concentration of fitting frequencies near 50 Hz is central to interpreting the thermal response, even though there are many fitting windows.

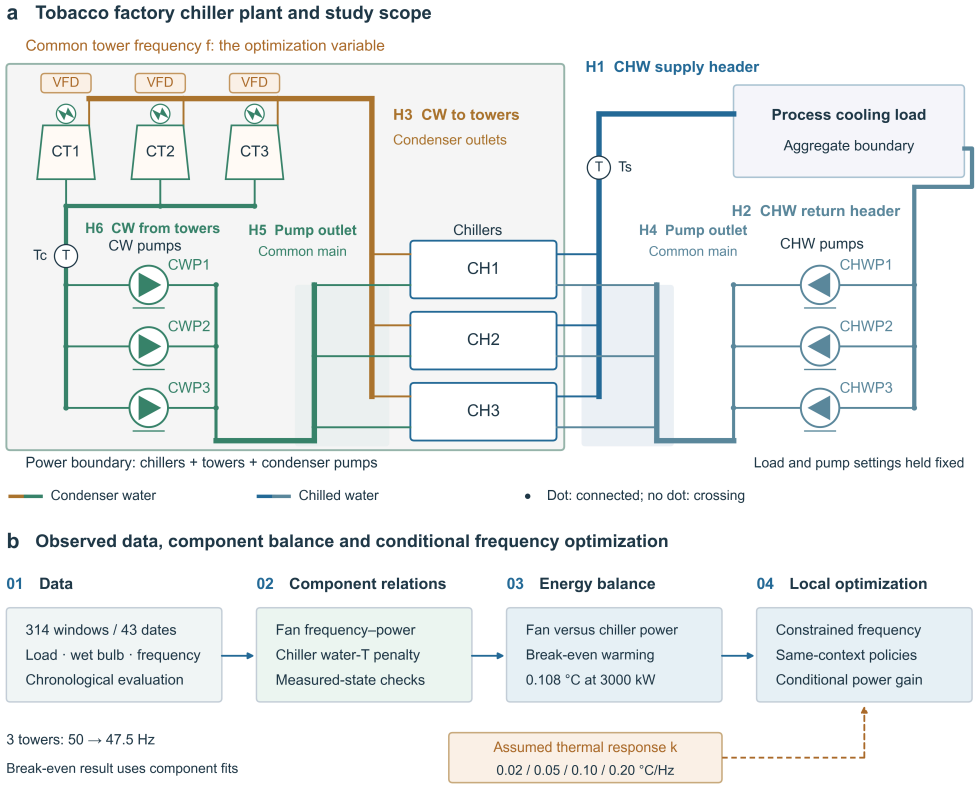


Figure 1. Common mains and frequency-optimization framework. (a) Thick pipes beside the chillers denote common mains. H1/H2 are chilled-water supply/return headers, and H4 collects chilled-water pump outlets. H3 carries condenser outlet water to towers; H6 collects tower outlet water to pump inlets; H5 collects condenser-pump outlets. Pump flows merge before distribution to chillers through the central mains. Dots mark connections; crossings without dots are unconnected. CT, CH, CWP and CHWP denote towers, chillers, condenser pumps and chilled-water pumps. Tc/Ts are measured on headers H6/H1, respectively. The outline marks the power boundary. Connections follow reference topology, not an as-built survey. (b) Component models determine break-even warming; assumed thermal response enters conditional optimization through the dashed orange branch. The 0.108 °C threshold refers to 3000 kW and three towers decreasing from 50 to 47.5 Hz

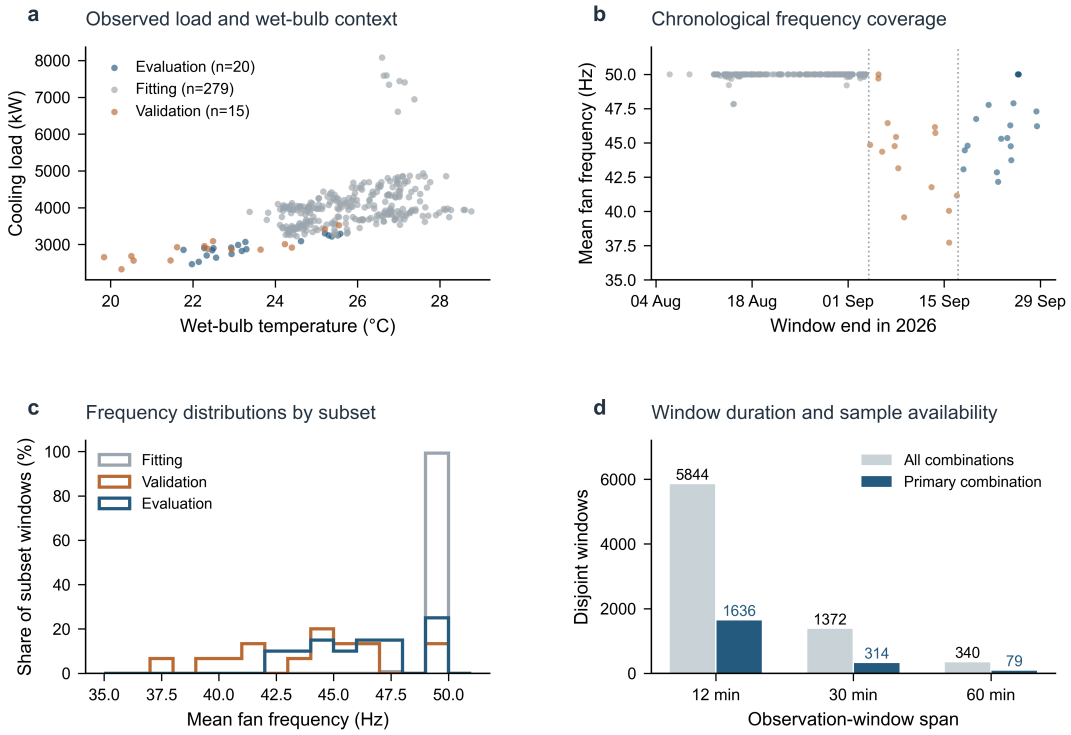


Figure 2. Observed operating coverage and sampling sensitivity. (a) All 314 primary-case windows in load and wet-bulb coordinates. (b) Mean achieved frequency over time; dotted lines separate fitting, validation and evaluation dates. (c) Frequency distributions normalized within each subset. (d) Disjoint windows under unchanged range thresholds at three observation spans. Gray, orange and blue represent fitting (279 windows), validation (15) and evaluation (20) in panels (a)–(c). No primary-case windows are subsampled

3. Component energy balance and optimization

3.1. Fan and chiller component relationships

The fan relationship uses a cubic frequency feature,

$$\widehat{P}_f = C_f \sum_{i=1}^{3} (f_i/50)^3. \tag{2}$$

The positive coefficient C_f is estimated by least squares through the origin on fitting windows. For a common frequency and n operating towers, the expression becomes $nC_f(f/50)^3$. This is an empirical aggregate relationship motivated by fan affinity behavior. Its coefficient describes measured electricity in this archive and must not be interpreted as a replacement for the motor nameplate rating. The individual frequency cubes are retained for factual fitting diagnostics, while common frequency scenarios use the aggregate form.

Chiller power is represented by a load normalized local regression,

$$\widehat{P}_c = q\{a_0 + a_T(T_c - 25) + a_Q(q - 3.5) + a_S(T_s - 9)\}, q = Q/1000. \tag{3}$$

Cooling load Q is in kW, T_c uses the H6 tower-return header measurement to represent condenser inlet temperature; T_s is measured on the H1 chilled-water supply header. The temperature coefficients satisfy $a_T \geq 0$ and $a_S \leq 0$. The load term adjusts the fit for the observed part-load regime. Because load is fixed in

the frequency scenarios, this regression is used for a local temperature sensitivity and not for optimizing plant load or extrapolating a global thermodynamic performance curve. The implied chiller sensitivity is

$$S_T(Q) = \partial \widehat{P}_c / \partial T_c = a_T Q / 1000. \tag{4}$$

Component errors are evaluated using measured water temperature. This deliberately conditions on a measured intermediate variable, and therefore does not validate a model that predicts water temperature under a changed fan frequency. A separate diagnostic couples a monotone tower approach map with the chiller model through rejected heat $Q + P_c$. Both logarithmic and linear approach families are fitted on fitting dates and compared on validation dates. This diagnostic asks whether the archive identifies the missing tower response. Its failure is retained in the assessment rather than absorbed into the fan or chiller error statistics.

3.2. Local thermal scenarios and break-even warming

For a window with observed common frequency f_0 and water temperature $T_{c,0}$, the local scenario is

$$T_c(f) = T_{c,0} + k(f_0 - f), k \geq 0. \tag{5}$$

The parameter k measures condenser water warming per hertz of frequency reduction. It can in reality depend on load, wet-bulb temperature, water flow and the evaluation horizon. Here, $k = 0.02$, 0.05, 0.10 and 0.20 °C/Hz are analyst specified scenarios used to expose sensitivity. They are not fitted estimates, a confidence interval or a validated physical range for this plant. Anchoring Equation (5) at an observed window likewise does not validate its slope.

At fixed context, the combined power change is

$$\Delta P_b(f) = S_T k(f_0 - f) + nC_f\{(f/50)^3 - (f_0/50)^3\}. \tag{6}$$

For a decrease to $f_1 < f_0$, the maximum warming that exactly consumes the fan electricity credit is

$$\Delta T_{BE} = \frac{nC_f\{(f_0/50)^3 - (f_1/50)^3\}}{S_T}. \tag{7}$$

Equation (7) is an energy balance conditional on the fitted component relations. It does not require claiming that the actual tower warming has already been measured. A warming smaller than the threshold produces a positive modeled net credit; a larger warming produces a negative credit within the local approximation. The criterion makes the required response measurement explicit and permits a practical comparison with sensor and operating variability.

3.3. Frequency solution and comparison policies

Differentiating Equation (6) gives the unconstrained local minimum. The feasible solution is

$$f^* = clip_F \sqrt{\frac{S_T k 50^3}{3nC_f}}. \tag{8}$$

The feasible interval F combines the retained equipment frequency range of 30–50 Hz, a local change of at most 2.5 Hz from f_0, and the temperature envelope. The condenser inlet research envelope is 18–32 °C, with approach at least 0.1 °C. These values are analysis bounds, not manufacturer approved or site authorized process limits. Wet-bulb temperature enters through the approach constraint and observed context. The analysis does not fit a reliable function $k(Q, T_{wb})$, and therefore does not claim to have established a complete weather dependent operating schedule.

Holding frequency, lowering it by 2.5 Hz, raising it by 2.5 Hz and targeting the fitting-period median approach are compared within the same feasible interval and component model. The median approach is 1.511

°C; this is an empirical comparison target, not a verified factory controller setting. The optimized solution is also evaluated for each window. The mean modeled power credit is the primary metric. The percentage is $100 \sum G_j / \sum \widehat{P}_{b,0,j}$, where $G_j = -\Delta P_{b,j}$. Equal window durations make this a consistent sampled-window comparison, but gaps and the conditional response assumption prevent conversion into seasonal energy savings.

3.4. Parameter sensitivity and evidence limits

Complete fitting dates are resampled with replacement 400 times. The component relations are refitted in each sample, retaining the observations within each selected date. This adapts the bootstrap principle [31] to a date block sensitivity analysis. The nominal scenario policy is then evaluated with each parameter draw without selecting a new policy in that draw. Reported bands are the 2.5th and 97.5th percentiles of the resulting model credit. They describe fitted parameter sensitivity conditional on the model and specified k. They omit unknown thermal response, model structure, sensor bias and counterfactual confounding.

The use of date blocks does not establish independence between dates. Nor does a prediction interval automatically provide a valid bound for an unobserved control effect. The unknown thermal response remains a structural limitation even when a component parameter band is narrow. Evidence is instead reported at its actual level: component fitting on observed states, derived break-even conditions, and optimization under an explicitly assumed response.

4. Results

4.1. Component accuracy and tower response identifiability

The fitted fan coefficient is 9.686 kW per normalized fan cube. Its date bootstrap percentile band is 9.658–9.717 kW. The chiller temperature coefficient a_T is 12.784, with a parameter band of 10.964–15.205 in the units of Equation (3). The other fitted chiller coefficients are $a_0 = 137.115$, $a_Q = -23.179$ and a_S effectively zero at its upper constraint. The boundary estimate for a_S cautions against using this fit to optimize chilled water temperature, which is outside the study scope.

Figure 3 and Table 2 report observed-state component errors, residual distributions and paired errors when the intermediate water state must be predicted. On the 20 evaluation windows, chiller RMSE is 11.24 kW and fan RMSE is 0.89 kW. The combined accounting-boundary RMSE is 11.54 kW, with a bias of −3.86 kW. These errors refer to measured condenser inlet temperature. When the missing temperature is instead predicted by the coupled logarithmic tower model, evaluation combined-power RMSE increases to 20.66 kW and condenser inlet temperature RMSE is 0.411 °C. Its frequency sensitivity reaches the zero lower bound. The linear family also places its frequency coefficient at the lower bound.

Table 2. Component validation using measured condenser inlet temperature

Subset	Chiller MAE kW	Chiller RMSE kW	Tower MAE kW	Tower RMSE kW	Boundary RMSE kW
Fitting	17.73	21.53	0.17	0.21	21.56
Validation	7.68	9.35	0.94	0.97	8.92
Evaluation	9.15	11.24	0.85	0.89	11.54

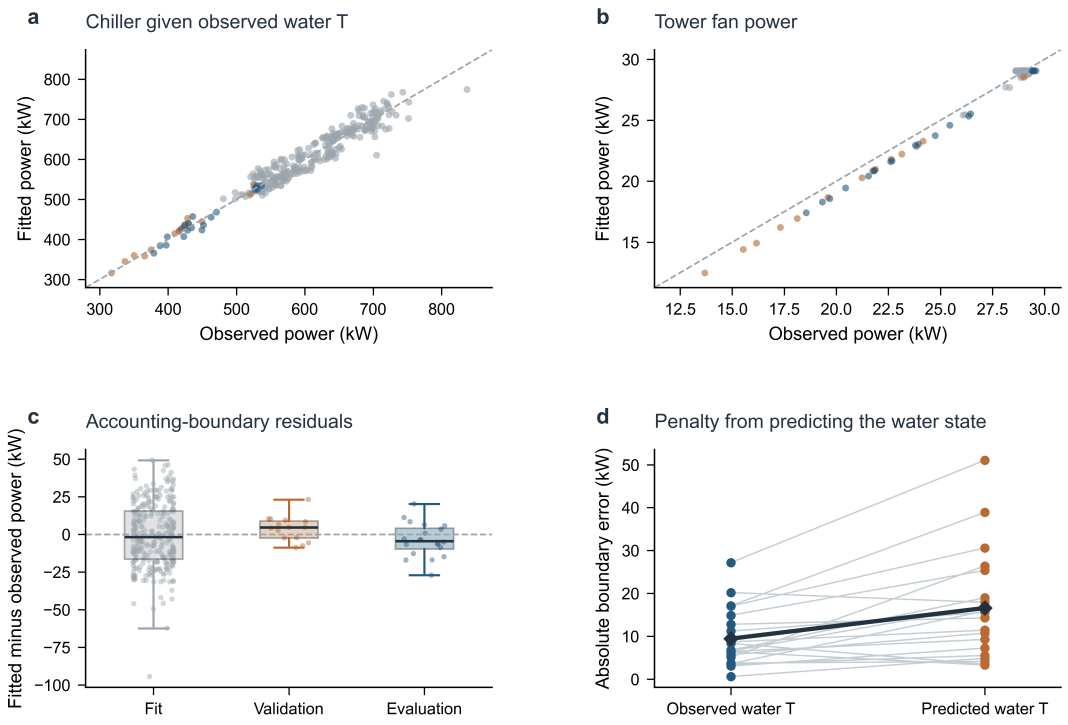


Figure 3. Observed-state component fit and the cost of predicting the intermediate water state. (a,b) Chiller and fan parity plots for all 314 windows, using the subset colors in Figure 2. Chiller fitting uses observed condenser inlet temperature. (c) Boundary residuals by subset, showing every window; boxes indicate medians and quartiles, with whiskers at 1.5 interquartile ranges and all points retained. Horizontal displacement only separates overlapping points. (d) Paired absolute boundary errors in the 20 evaluation windows when water temperature is observed or supplied by the coupled logarithmic tower model. Thin lines connect the same window; black diamonds mark the two means. These are factual prediction diagnostics, not an intervention validation

The zero tower coefficient is evidence of inadequate response identification under this model and sampling regime. It is not evidence that fan frequency has no physical effect. Only a 2.18 Hz mean-frequency span occurs in fitting windows, while the later subsets contain materially lower frequencies. Temperature, weather and existing feedback behavior change together. For this reason, the coupled model is not used to claim an identified optimum; Equations (5)–(8) instead show the conditional result and the measurement on which it depends.

4.2. Fan electricity credit and break-even water warming

The fitted relationship gives a total three-tower power of 29.06 kW at 50 Hz. Reducing common frequency to 47.5 Hz saves 4.14 kW in the fan model, while reducing to 45 Hz saves 7.87 kW. These are component model estimates, not measured responses to a newly applied frequency command. The corresponding chiller temperature penalty rises with cooling load through Equation (4).

At 3000 kW load, the estimated chiller penalty is 38.35 kW per degree Celsius. The 4.14 kW credit from a 2.5 Hz reduction can therefore cover only 0.108 °C of water warming. At 4500 kW, the allowable warming falls to 0.072 °C. Table 3 and Figure 4 quantify this relation. At the same loads, a 5 Hz reduction provides a

larger fan credit but can tolerate only 0.205 and 0.137 °C of warming, respectively. A larger frequency reduction consequently does not eliminate the need for a precise thermal response estimate.

Table 3. Conditional break-even temperatures for three towers starting at 50 Hz

Cooling load kW	Chiller penalty kW per °C	Warming for 2.5 Hz decrease °C	Warming for 5 Hz decrease °C
2500	31.96	0.130	0.246
3000	38.35	0.108	0.205
3500	44.74	0.093	0.176
4000	51.14	0.081	0.154
4500	57.53	0.072	0.137

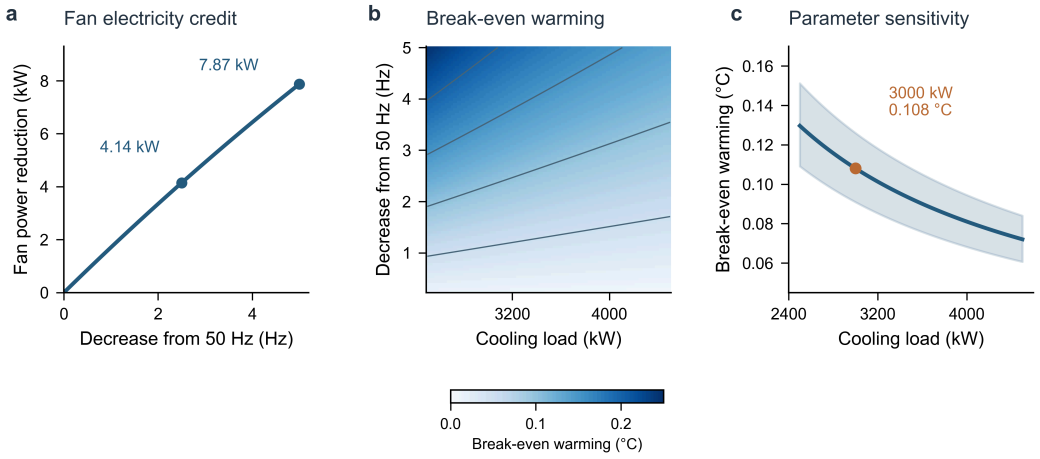


Figure 4. Conditional break-even warming from the component energy balance. (a) Modeled three-fan power credit for decreases from 50 Hz. (b) Derived allowable water warming across load and frequency decrease; contours mark 0.05 °C increments. (c) A 2.5 Hz decrease with 2.5th–97.5th percentile component-parameter bands from 400 fitting-date resamples. The 3000 kW point allows about 0.108 °C of warming. The map and bands do not estimate the actual tower warming

4.3. Conditional optimum and policy comparison

At 3000 kW and 50 Hz, the marginal thermal sensitivity that balances the power derivative is approximately 0.0455 °C/Hz. A smaller local warming sensitivity favors reducing frequency; a larger sensitivity can favor raising frequency until a bound is reached. Figure 5 combines the opposing component contributions with a load–sensitivity map of the conditional optimum and the marginal direction boundary. The optimum follows from the component slopes rather than the complexity of the numerical solver. Equation (8) also shows why higher cooling load increases the preferred frequency when k and other conditions remain fixed.

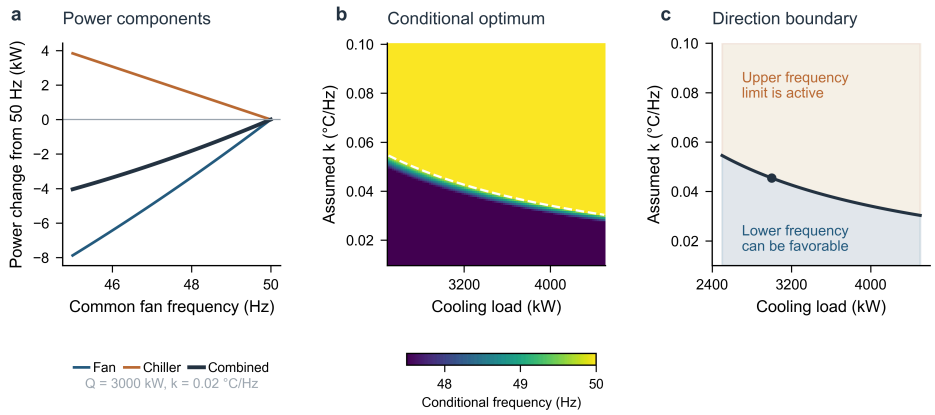


Figure 5. Conditional optimization mechanism and direction boundary. (a) Fan, chiller and combined power changes at Q=3000 kW and assumed k=0.02◦C/Hz. (b) Conditional local optimum for a 50 Hz starting frequency, constrained to 47.5–50 Hz; the dashed line is the marginal break-even sensitivity. (c) The same boundary distinguishes a potentially beneficial reduction from an active upper-frequency limit. The thermal sensitivity is an assumed axis throughout, not an empirically identified operating schedule

Table 4 reports the 20 later evaluation contexts. At $k = 0.02$ °C/Hz, the local optimum lowers frequency in all 20 windows and provides a mean modeled credit of 1.70 kW, or 0.315%. At $k = 0.05$, 0.10 and 0.20 °C/Hz, the optimum raises frequency in 15 windows and leaves the remaining five at their upper frequency. Mean modeled credits are 0.55, 3.86 and 10.50 kW. The direction change is a material result: a generic instruction to slow every tower is inconsistent with the energy balance once the chiller temperature penalty becomes sufficiently large.

Table 4. Local optimization under explicitly assumed thermal sensitivities

Assumed k °C per Hz	Changed windows	Mean credit kW	Credit percent	Parameter band kW	Median frequency Hz
0.02	20 of 20	1.70	0.315	1.35 to 1.97	43.75
0.05	15 of 20	0.55	0.101	0.07 to 1.17	48.75
0.10	15 of 20	3.86	0.717	2.92 to 5.12	48.75
0.20	15 of 20	10.50	1.948	8.61 to 13.01	48.75

The bands in Table 4 are conditional parameter sensitivity bands, not confidence intervals for realized savings. All candidate temperatures satisfy the stated research envelope within the scenario equations. This mathematical feasibility is not a measurement of constraint violation probability or duration under plant control. No adjustment commands have been transmitted or verified by these calculations.

The fixed direction comparisons reinforce the dependence on thermal response. At $k = 0.10$ °C/Hz, uniformly lowering frequency by 2.5 Hz gives a mean modeled loss of 5.80 kW, whereas the optimized or uniformly raised feasible policy gives a credit of 3.86 kW. The training median approach target gives 1.41 kW. At $k = 0.20$, uniform reduction gives a 15.16 kW loss, while the conditional optimum gives a 10.50 kW credit. Conversely, at $k = 0.02$, raising frequency increases modeled power by 1.45 kW. Figure 6 compares these policies using identical contexts, bounds and component parameters.

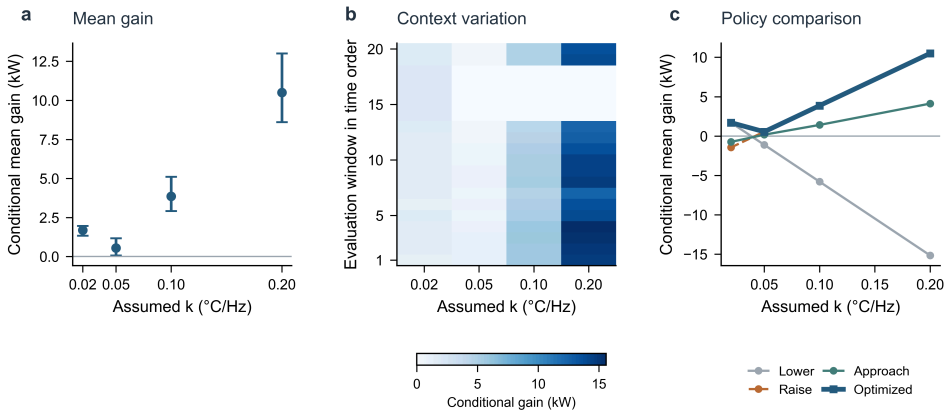


Figure 6. Conditional gains and same-context policy comparisons. (a) Mean gains over 20 evaluation windows; bars show 2.5th–97.5th percentile component-parameter sensitivity from 400 fitting-date resamples. (b) All 20 windows in chronological order across four assumed sensitivities, without averaging away window heterogeneity. (c) Policies use the same contexts, model and frequency/temperature bounds. Optimized and raised-frequency results overlap in three scenarios. All gains depend on assumed k and are not measured savings

4.4. Sampling and uncertainty sensitivity

Window length materially affects the available evidence. Keeping the same range thresholds but using three, six or eleven observations yields 5,844, 1,372 and 340 disjoint windows across all combinations. These spans are 12, 30 and 60 minutes, respectively. The primary case counts fall from 1,636 to 314 and then 79, and the number of represented primary case dates falls from 54 to 43 and then 22. Longer screening does not automatically solve response identification; it can further concentrate the sample around nearly constant operation.

The smallest conditional credit, 0.55 kW at $k = 0.05$, is much smaller than the 11.54 kW accounting-boundary RMSE. A comparison of these magnitudes does not by itself calculate the uncertainty of a paired control effect, because errors may be correlated. It does establish that the reported absolute fitting accuracy cannot substantiate a sub-kilowatt physical saving. More importantly, varying the unmeasured k changes the preferred direction. Reducing uncertainty in that parameter is therefore more consequential for deployment than refining the last decimal place of the optimizer.

5. Discussion

5.1. Implications for tobacco factory operation

The practical output is a temperature measurement target attached to an energy tradeoff. For example, at 3000 kW, a three-tower reduction from 50 to 47.5 Hz is attractive in the fitted balance only if the resulting condenser inlet warming stays below approximately 0.108 °C. At higher load, the allowable rise is smaller. An operator can use this threshold to plan a controlled trial and to judge whether measurement uncertainty is too large to distinguish the alternatives. The numerical threshold is conditional on the component model, so it should be recalculated after new component measurements or equipment changes.

The tobacco production setting also limits what can be optimized independently. Chilled water supply requirements originate downstream of the cold source. A fan experiment must therefore retain existing plant protection and the agreed cooling service, and any process environmental evaluation requires the corresponding workshop measurements. The present results do not show improved product quality, protected humidity or reduced production disturbance. They supply a water side energy comparison that can be included in a wider factory validation program.

The analysis indicates that a uniform low-frequency policy is not justified by fan savings alone. It also does not establish that raising frequency is always preferable. The scenario producing the largest credit, 10.50 kW, assumes the largest thermal sensitivity. Presenting that value without its assumption would overstate the evidence. The appropriate operational conclusion is to measure the response that decides between the policies, rather than choose the most favorable assumed percentage.

5.2. Validation needed for implemented optimization

A useful next experiment fixes the same equipment combination and pump settings and alternates an established fan frequency with a small permitted change. The site must approve the actual frequency and temperature limits. Both lower and higher frequency perturbations should be represented where allowed. The period after each adjustment must be long enough for the identified thermal response, rather than being fixed to one six minute sample by convenience. Repeated baseline, changed-frequency and restored-baseline periods can help detect load or weather drift, but cannot remove every confounder without a suitable design.

The experiment should record command issue time, achieved frequency, water temperatures, flows and separate chiller and tower powers. Temperature calibration and synchronization are particularly important because the break-even rise can be below 0.1 °C. Cooling load and wet-bulb strata should be represented repeatedly across operating dates. After fitting a context dependent response $k(Q, T_{wb}, G)$ or an appropriate dynamic tower model, freeze the optimizer and comparison policies before a new evaluation period. Report integrated energy over complete matched periods, supply-water deviations, adjustment counts and any intervention interruptions. Such a result would support an implemented control paper; the current scenario analysis supplies its quantitative design targets.

The study remains limited by one primary combination, a small later-window sample, a strong shift in frequency distribution, and unmeasured counterfactual thermal response. The component regression can also contain sensor and operating confounding. Date resampling cannot correct those structural limitations. Replication in other fixed combinations and independent response measurements are needed before transferring either the numerical coefficients or the calculated frequencies to wider operation.

6. Conclusions

For the studied fixed combination in a tobacco factory chiller plant, the fan and chiller energy balance gives a concrete limit on beneficial frequency reduction. The fitted three-tower fan model estimates credits of 4.14 kW for 50 to 47.5 Hz and 7.87 kW for 50 to 45 Hz. At 2500–4500 kW cooling load, the former credit can cover only 0.130–0.072 °C of condenser water warming. At 3000 kW, its break-even rise is approximately 0.108 °C. These values identify the response resolution required to assess a proposed reduction.

On 20 later observed windows across nine dates, chiller and fan RMSE values are 11.24 and 0.89 kW when measured condenser water temperature is supplied. This observed-state accuracy does not identify the temperature effect of a changed frequency. The coupled tower models fail to identify a reliable positive

cooling response from the concentrated fitting actions, so an unconditional weather dependent optimal frequency or measured saving cannot be reported from this archive.

Under explicitly assumed thermal sensitivities of 0.02–0.20 °C/Hz, local optimization gives conditional mean credits of 0.55–10.50 kW, corresponding to 0.10%–1.95% of the modeled chiller, tower and condenser-pump boundary. The preferred direction changes from lower to higher frequency as the thermal penalty increases. At 0.10 °C/Hz, uniform reduction gives a 5.80 kW modeled loss while the conditional optimum gives a 3.86 kW credit. The engineering conclusion is therefore that tower frequency optimization must balance fan electricity against a measured chiller temperature penalty. The present study quantifies that balance and its validation targets; it does not claim achieved closed loop energy savings.

Data and code availability

The study package contains sample construction code, fitted parameters, numerical tables and Python sources for every figure. Source hashes and the inclusive data cutoff are recorded. The industrial archive is retained locally and is not publicly redistributed. Reproduction requires authorized access to the recorded snapshot. No control command interface is included.

Funding

The research is supported by 2025 Hebei Zhongyan Industry Co., Ltd. Technology Project: "Research on Precision Control and Supply Quality Optimization of Power Energy for Energy-Consuming Key Equipment" (HBZY2025A029)

References

[1] He, Y., Wang, H., & Jiang, J. (2022). Research on temperature and humidity decoupling control of process air conditioning in cigarette factory. In *2022 IEEE 6th Information Technology and Mechatronics Engineering Conference (ITOEC)* (pp. 1062-1066). IEEE. https://doi.org/10.1109/ITOEC53115.2022.9734444

[2] Zhou, Z., Zhang, Y.-g., Xie, D., Luo, X., & Yao, M.-y. (2025). Simulation and optimization design of air distribution in a cigarette production factory. *Indoor and Built Environment, 34*(1), 251-263. https://doi.org/10.1177/1420326X241283529

[3] Wang, S., & Ma, Z. (2008). Supervisory and optimal control of building HVAC systems: A review. *HVAC& R Research, 14*(1), 3-32. https://doi.org/10.1080/10789669.2008.10390991

[4] Lu, L., Cai, W., Soh, Y. C., Xie, L., & Li, S. (2004). HVAC system optimization—condenser water loop. *Energy Conversion and Management, 45*(4), 613-630. https://doi.org/10.1016/S0196-8904(03)00181-X

[5] Jin, G.-Y., Cai, W.-J., Lu, L., Lee, E. L., & Chiang, A. (2007). A simplified modeling of mechanical cooling tower for control and optimization of HVAC systems. *Energy Conversion and Management, 48*(2), 355-365. https://doi.org/10.1016/j.enconman.2006.07.010

[6] Cao, Y., Wang, C., Wang, S., Fu, X., & Ming, X. (2024). Energy modeling and optimization of building condenser water systems with all-variable speed pumps and tower fans: A case study. *Building Simulation, 17*(7), 1085-1111. https://doi.org/10.1007/s12273-024-1123-8

[7] Ma, K., Liu, M., & Zhang, J. (2021). Online optimization method of cooling water system based on the heat transfer model for cooling tower. *Energy, 231*, 120896. https://doi.org/10.1016/j.energy.2021.120896

[8] Chen, X., Guan, L., Yang, C., Ge, P., & Xia, J. (2025). A novel optimal control method for building cooling water systems with variable speed condenser pumps and cooling tower fans. *Buildings, 15*(19), 3568. https://doi.org/10.3390/buildings15193568

[9] Stabat, P., & Marchio, D. (2004). Simplified model for indirect-contact evaporative cooling-tower behaviour. *Applied Energy, 78*(4), 433-451. https://doi.org/10.1016/j.apenergy.2003.09.004

[10] Singh, K., & Das, R. (2017). Exergy optimization of cooling tower for HGSHP and HVAC applications. *Energy Conversion and Management, 136*, 418-430. https://doi.org/10.1016/j.enconman.2017.01.024

[11] Wu, Z., Lu, Z., Zhang, B., He, C., Chen, Q., Yu, H., & Ren, J. (2022). Stochastic bi-objective optimization for closed wet cooling tower systems based on a simplified analytical model. *Energy, 250*, 123703. https://doi.org/10.1016/j.energy.2022.123703

[12] Fan, Z., Di, Y., Zhang, Q., Chen, H., Li, Y., Luo, M., & Gao, Y. (2026). Data-driven modeling method of cooling tower systems: Holistic, dynamic, and explainable. *Energy, 353*, 141001. https://doi.org/10.1016/j.energy.2026.141001

[13] Liang, X., Liu, Y., Chen, S., Li, X., Jin, X., & Du, Z. (2025). Physics-informed neural network for chiller plant optimal control with structure-type and trend-type prior knowledge. *Applied Energy, 390*, 125857. https://doi.org/10.1016/j.apenergy.2025.125857

[14] Zhao, Z., Li, Y., Salsbury, T. I., & House, J. M. (2022). Global self-optimizing control with data-driven optimal selection of controlled variables with application to chiller plant. *Journal of Dynamic Systems, Measurement, and Control, 144*(2), 021008. https://doi.org/10.1115/1.4052395

[15] Afram, A., & Janabi-Sharifi, F. (2014). Theory and applications of HVAC control systems – A review of model predictive control (MPC). *Building and Environment, 72*, 343-355. https://doi.org/10.1016/j.buildenv.2013.11.016

[16] Killian, M., & Kozek, M. (2016). Ten questions concerning model predictive control for energy efficient buildings. *Building and Environment, 105*, 403-412. https://doi.org/10.1016/j.buildenv.2016.05.034

[17] Drgoňa, J., Arroyo, J., Cupeiro Figueroa, I., Blum, D., Arendt, K., Kim, D., Ollé, E. P., Oravec, J., Wetter, M., Vrabie, D. L., & Helsen, L. (2020). All you need to know about model predictive control for buildings. *Annual Reviews in Control, 50*, 190-232. https://doi.org/10.1016/j.arcontrol.2020.09.001

[18] Kim, S., Shin, H., Mun, J., Lee, J. H., Doh, Y., & Park, C.-S. (2026). Stochastic model predictive control for chiller systems using machine-learning models with quantified prediction uncertainty. *Energy and Buildings, 369*, 117914. https://doi.org/10.1016/j.enbuild.2026.117914

[19] Fan, C., & Zhou, X. (2023). Model-based predictive control optimization of chiller plants with water-side economizer system. *Energy and Buildings, 278*, 112633. https://doi.org/10.1016/j.enbuild.2022.112633

[20] Chen, D., Gong, Y., Chen, J., & He, R. (2026). The evolution and future of advanced control strategies for chiller plant sequence and optimal loading in buildings: A review of modern control theory and artificial intelligence algorithms. *Energy and Buildings, 364*, 117578. https://doi.org/10.1016/j.enbuild.2026.117578

[21] Shmueli, G. (2010). To explain or to predict? *Statistical Science, 25*(3), 289-310. https://doi.org/10.1214/10-STS330

[22] Schoukens, J., & Ljung, L. (2019). Nonlinear system identification: A user-oriented road map. *IEEE Control Systems, 39*(6), 28-99. https://doi.org/10.1109/MCS.2019.2938121

[23] Valenzuela, P. E., Ebadat, A., Everitt, N., & Parisio, A. (2020). Closed-loop identification for model predictive control of HVAC systems: From input design to controller synthesis. *IEEE Transactions on Control Systems Technology, 28*(5), 1681-1695. https://doi.org/10.1109/TCST.2019.2917675

[24] Uematsu, R., Masuda, S., & Kano, M. (2022). Closed-loop identification of plant and disturbance models based on data-driven generalized minimum variance regulatory control. *Journal of Process Control, 115*, 197-208. https://doi.org/10.1016/j.jprocont.2022.05.002

[25] Ssembatya, M., Baltazar, J.-C., & Claridge, D. E. (2025). Evaluating inverse modeling methods for measurement and verification of chiller energy efficiency measures. *Applied Energy, 378*, 124805. https://doi.org/10.1016/j.apenergy.2024.124805

[26] Heo, Y., & Zavala, V. M. (2012). Gaussian process modeling for measurement and verification of building energy savings. *Energy and Buildings, 53*, 7-18. https://doi.org/10.1016/j.enbuild.2012.06.024

[27] Zaw, K., Lik, C. C., & Poh, T. K. (2026). Chiller plant optimization for carbon-neutral cooling: Field case studies and energy performance analysis. *Applied Thermal Engineering, 303*, 132459. https://doi.org/10.1016/j.applthermaleng.2026.132459

[28] Zhu, S., Lv, S., Wang, W., & Cui, M. (2024). Toward optimal design of a factory air conditioning system based on energy consumption prediction. *Processes, 12*(12), 2615. https://doi.org/10.3390/pr12122615

[29] Blum, D., Arroyo, J., Huang, S., Drgoňa, J., Jorissen, F., Walnum, H. T., Chen, Y., Benne, K., Vrabie, D., Wetter, M., & Helsen, L. (2021). Building optimization testing framework (BOPTEST) for simulation-based benchmarking of control strategies in buildings. *Journal of Building Performance Simulation, 14*(5), 586-610. https://doi.org/10.1080/19401493.2021.1986574

[30] Stull, R. (2011). Wet-bulb temperature from relative humidity and air temperature. *Journal of Applied Meteorology and Climatology, 50*(11), 2267-2269. https://doi.org/10.1175/JAMC-D-11-0143.1

[31] Efron, B. (1979). Bootstrap methods: Another look at the jackknife. *The Annals of Statistics, 7*(1), 1-26. https://doi.org/10.1214/aos/1176344552